Study of glass formation and crystallization kinetics in a 2D metal halide perovskite using ultrafast calorimetry

Akash Singh,[1,2] Yongshin Kim,[1,2] Reece Henry,[3] Harald Ade,[3] David B. Mitzi[*,1,4]*

[1]Department of Mechanical Engineering and Materials Science, Duke University, Durham, North Carolina 27708, United States

[2]University program in Materials Science and Engineering, Duke University, Durham, North Carolina 27708, United States

[3]Organic and Carbon Electronics Laboratory (ORaCEL), Department of Physics, North Carolina State University, Raleigh, NC, 27695.

[4]Department of Chemistry, Duke University, Durham, North Carolina 27708, United States

[*]Corresponding author: david.mitzi@duke.edu

Abstract

While crystalline 2D metal halide perovskites (MHPs) represent a well-celebrated semiconductor class, with ensuing applications in the fields of photovoltaics, emitters, and sensors, the recent discovery of glass formation in an MHP opens many new opportunities associated with reversible glass-crystalline switching, with each state offering distinct optoelectronic properties. However, the previously reported [S-(−)-1-(1-naphthyl)ethylammonium]$_2$PbBr$_4$ perovskite is a strong glass former with sluggish glass-crystal transformation timescales, pointing to a need for glassy MHPs with a broader range of compositions and crystallization kinetics. Herein we report glass formation in low melting temperature 1-MeHa$_2$PbI$_4$ (1-MeHa = 1-methyl-hexylammonium) using ultrafast calorimetry, thereby extending the range of MHP glass formation across a broader range of organic (fused ring to branched aliphatic) and halide (bromide to iodide) compositions. The importance of a slight loss of organic and hydrogen iodide components from the MHP in stabilizing the glassy state is elucidated. Furthermore, the underlying kinetics of glass-crystal transformation, including activation energies, crystal growth rate, Angell plot, and fragility index is studied using a combination of kinetic, thermodynamic, and rheological modeling techniques. An inferred fast crystal growth rate of 0.21 m/s for 1-MeHa$_2$PbI$_4$ shows promise toward suitability in extended application spaces, for example in metamaterials, nonvolatile memory, and optical and neuromorphic computing devices.

Keywords: Metal halide perovskite, glass, ultrafast calorimetry, kinetics, phase change materials

Introduction

Hybrid metal halide perovskite (MHP) systems have recently been introduced into the family of glass-forming semiconductors.[1, 2] The discovery of an accessible glass state, as well as the demonstration of reversible switching between the glassy and crystalline states in a MHP, has the potential to expand the associated application space beyond the conventionally celebrated fields of photovoltaics,[3-5] emitters,[6] and detectors.[7] So far, glass formation in MHPs has been restricted to an exemplary chiral lead bromide-based system, [S-(−)-1-(1-naphthyl)ethylammonium]$_2$PbBr$_4$ (abbreviated as SNPB)[1]. In this system, laboratory scale cooling rates of as low as 20°C/min—e.g., achievable using a conventional differential scanning calorimeter (DSC)—can lead to nominally complete *in-situ* glass formation. However, the low critical cooling rate requirement (minute-scale ordering timescale) and higher glass forming ability (defined by the Turnbull criteria[8]—i.e., ratio of glass transition temperature, T_g, and melting temperature, T_m) result in a relatively sluggish glass-crystal transformation with activation energy requirement of as high as ~350 kJ/mol.[9] Hence, there is interest in exploring other MHP compositions that can undergo vitrification and that show different degrees of glass forming abilities. Success in this domain would expand the family of MHP glass formers while also helping to set up design principles that connect the diverse MHP compositional space[10, 11] with their tendency to form a glass. Moreover, small ordering timescales (microseconds to sub-nanoseconds)[12, 13] during glass crystallization may prospectively enable applications wherein fast switching is a requirement, for example in memory,[13, 14] neuromorphic computing,[14, 15] metamaterials,[16] and photonic devices.[16, 17]

The foremost requirement for a hybrid MHP to enable glass formation and reversible glass-crystal switching is for the hybrid to have a T_m lower than its degradation temperature (typically, T_d ~200°C),[1, 18] which ensures a relatively stable working regime for the vitrification and devitrification processes. From within the limited set of two-dimensional (2D) MHP systems available to date with T_m <200°C, we selected a representative member from this family with chemical formula [1-methyl-hexylammonium]$_2$PbI$_4$ (abbreviated as 1-MeHa$_2$PbI$_4$), which has one of the lowest reported T_m values of ~164°C.[1, 19, 20] Melt processing of 1-MeHa$_2$PbI$_4$ into films and monoliths generally leads to a crystalline phase, as demonstrated in our previous reports.[1, 19] Due to high propensity toward crystallization and facile reordering kinetics for the 1-MeHa$_2$PbI$_4$ melt, crystallization cannot be averted when cooled at rates supported by conventional calorimeters (up to 50°C/min).[1, 19] On the other hand, ultrafast ("flash") calorimetry (heating/cooling rates >1000 °C/s)[21] has previously been used to study glass formation and cold crystallization phenomenon in metals,[22, 23] organics,[24] polymers,[25] and chalcogenides.[26-29] Recently, we used flash-DSC to explore the kinetic control of solid-solid polymorphic structural transitions in a MHP.[30] In the current study, we explore the utility of this technique for glass formation in 1-MeHa$_2$PbI$_4$. Through this study, we demonstrate the first glass-forming iodide-based MHP and associated weaker glass forming character relative to previously studied SNPB perovskite. The study further uncovers the importance of organic and hydrogen halide loss during the heating process for MHPs, in terms of stabilizing the glass phase. We connect the temperature-dependent viscosity of MHPs with glass formation, by performing a comparative study of 1-MeHa$_2$PbI$_4$ and SNPB. Finally, the rheological,

kinetic and thermodynamic characteristics for 1-$MeHa_2PbI_4$ are evaluated by means of numerical modelling to obtain the fragility index, Angell plot, activation energy for crystallization, and crystal growth rates, to shape an initial understanding of the underlying kinetics of glass formation and subsequent crystallization for known and prospective MHPs.[26-28] Ultrafast calorimetry is thereby introduced as a versatile approach to study glass formation and crystallization phenomenon within tunable MHPs and related hybrid systems, as well as in terms of tailoring switching within these systems.

Results and Discussion

Glass formation and cold crystallization: In an initial attempt to produce a glass by employing higher cooling rates, a melt of 1-$MeHa_2PbI_4$ sandwiched between two soda-lime glass substrates (maintained at 190 °C) was rapidly immersed in liquid nitrogen; however, the manual handling of the samples didn't result in vitrification and instead a family of repeating crystalline peaks appear in the X-ray diffraction (XRD) analysis (Figure S1). Hence, in the current study, we adopt ultrafast ("flash") calorimetry, which can support cooling rates of as high as 6,000 °C/s, as an alternative route to vitrify the 1-$MeHa_2PbI_4$ melt, while simultaneously providing a pathway to track the underlying kinetics of glass formation.[21] As a first step to using the ultrafast calorimeter, a crystal (~100 ng) of 1-$MeHa_2PbI_4$ prepared through slow cooling (details in Methods section) was melted above the T_m at 180 °C for 1.5 seconds to ensure effective thermal contact with the heater region of the flash-DSC UFS-1 chip. After this step, the melt was cooled at 6000 °C/s (maximum achievable in the temperature region of interest). Notably, a cooling rate of as high as 6000 °C/s does not vitrify the melt and instead results in crystallization exotherms (red curve, Figure 1a), revealing the ultrafast ordering kinetics in 1-$MeHa_2PbI_4$ and pointing to the need for an even higher cooling rate (>6000 °C/s) to access the glassy state in this system. The observation of multiple exothermic peaks during the cooling run may signify peak splitting under rapid cooling, suggesting a combination of melt crystallization processes and associated kinetics, owing to the hybrid nature of the organic-inorganic MHPs.[30, 31] Upon reheating (250 °C/s), an endothermic melting peak is observed at ~160 °C (red curve, Figure 1b). Interestingly, upon repeating the same measurement, i.e., cooling and heating cycles, we start to observe a gradual reduction in exothermic crystallization peak intensities during cooling (Figure 1a) and the emergence of a single cold crystallization peak (T_p) at 45 °C on subsequent heating (Figure 1b) of the sample. This behavior gets more pronounced with repeated cycles and, after a few iterations, the cooling curve becomes essentially a straight line (characteristic of melt quenching or glass formation)[1] and the formed glass crystallizes only during the subsequent heating run (referred as cold crystallization). Though evidence of melt quenching and cold crystallization is present, we did not observe any glass transition region using the thermal cycle in Figure 1, which otherwise is a characteristic of many glass forming systems.[32] Such a transition is often absent in DSC analysis for poor glass forming systems, e.g. germanium-antimony-tellurium (GST), which instead is extracted through rheological and kinetic modeling.[26] However, 1-$MeHa_2PbI_4$ does show the signature of a glass transition during the melt quenching process when the measured temperature range is extended.

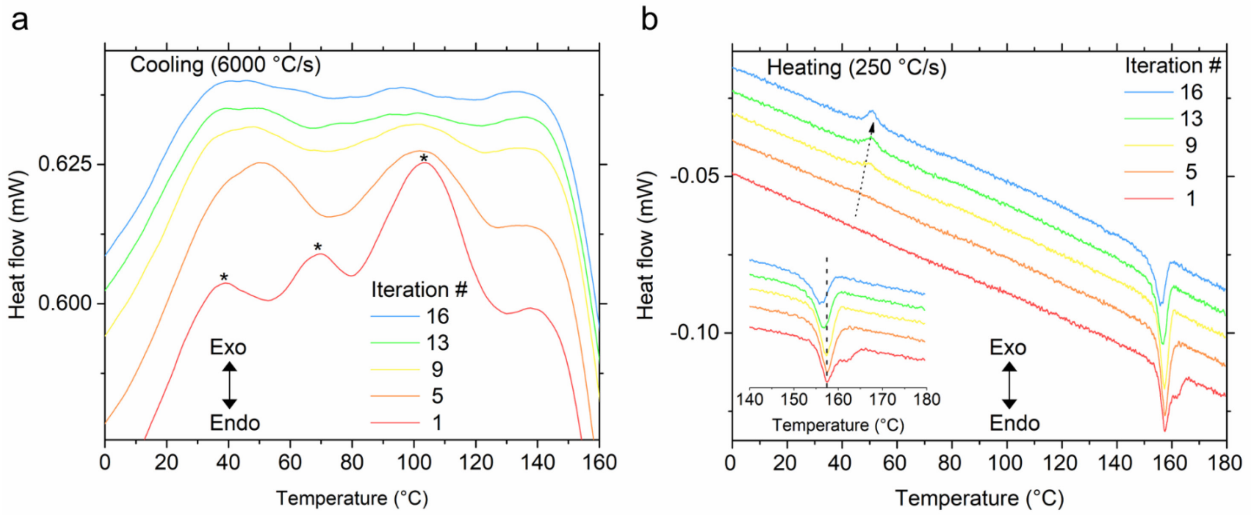

Figure 1. *Glass formation and cold crystallization in 1-MeHa$_2$PbI$_4$ perovskite, as measured using flash-differential scanning calorimetry (flash-DSC) with cooling and heating curves obtained at 6000°C/s and 250°C/s, respectively. On cooling the melt of the material, exothermic crystallization peaks are observed (star marks on the red curve in* ***a****) with no cold crystallization in the subsequent heating run (red curve in* ***b****), suggesting no glass formation. However, after multiple heat-cool iterations, a small amount of organic and hydrogen iodide loss can result in quenching of crystallization peaks (e.g., blue curve in* ***a****) with subsequent emergence of a cold crystallization peak in the next heating run (e.g., blue curve in* ***b*** *and marked with dashed arrow). The inset of the panel* ***b)*** *also suggests slight reduction in melting temperature over multiple iterations of heat-cool cycles (confirmed from conventional DSC in Figure S2). The vertical axis is only for representation of scale of magnitude i.e., the curves are vertically offset for clarity.*

To access the possible glass transition regime, we performed similar heat-cool iterations on another 1-MeHa$_2$PbI$_4$ crystal using a new UFS-1 chip with a reduced cooling rate (3000 °C/s), which in turn allows the collection of meaningful data points in the lower temperature range, i.e., down to -40 °C. Melt quenching (disappearance of exothermic crystallization peaks) is observed after 31 heat-cool iterations, which is subsequently followed by an offset in baseline—i.e., characteristic of a glass transition (Figure 2a).[33] The glass transition regime continues to be seen in essentially the same temperature range (-40 °C to 40 °C) over 90 iterations, with characteristic temperature T_g = 15.5 °C obtained through the mid-point height method and recorded at a cooling rate of 3000 °C/s. [33, 34] For comparison, an empty UFS-1 chip cooled at 3000 °C/s doesn't show such a shift in baseline (Figure S3). The higher number of heat-cool iterations required to effectively quench the melt to a glass state (31 as opposed to 16 for the first measurement) in this subsequent study is likely due to the bigger size (i.e., smaller surface area to volume ratio) of the crystal employed in the new measurement (Figure S4), as well as the application of reduced cooling rates (3000 °C/s as opposed to 6000 °C/s). Further lowering of the cooling rate allows access to data points at even lower temperatures, which helped obtain a well-defined T_g (Figure S5) with distinct baselines,

indicative of a change in specific heat capacity (C_p) on transitioning from a supercooled liquid to a solidified glass.

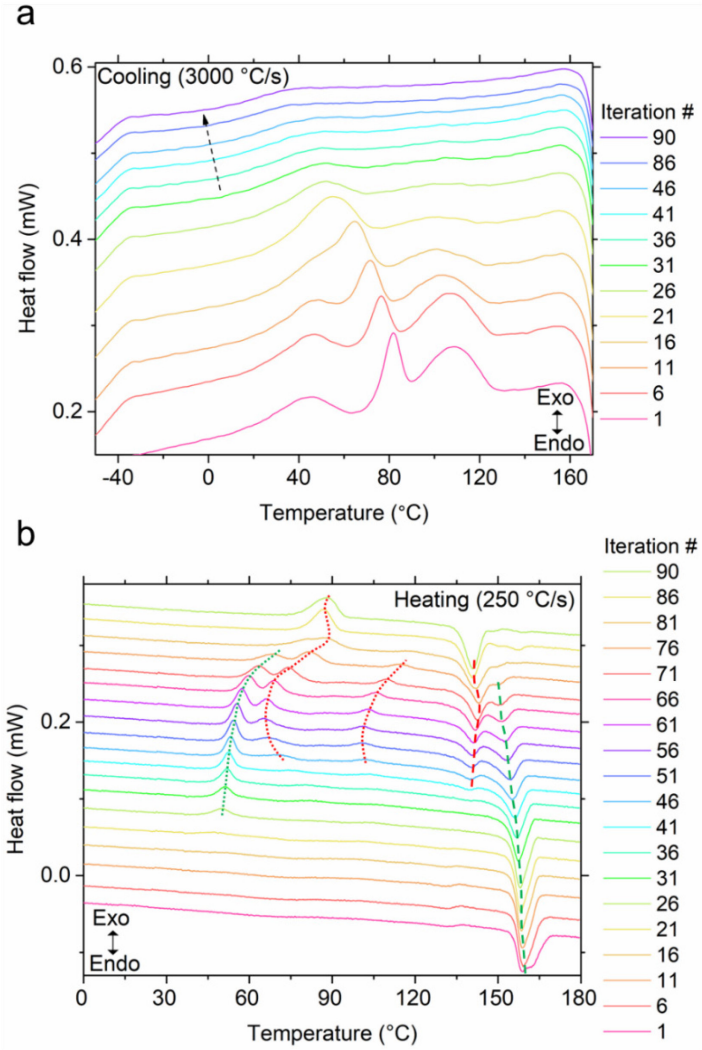

Figure 2. *Glass formation and cold crystallization in 1-MeHa$_2$PbI$_4$ perovskite over an extended number of iterations. After an initial few iterations (31) on cooling the melt at 3000°C/s (to access the lower temperature range), exothermic crystallization peaks of the 1-MeHa$_2$PbI$_4$ phase are essentially quenched* ***a****), with emergence of a cold crystallization peak (guided by the green dotted line) and its melting (guided by the green dashed line) in the subsequent heating run,* ***b****). With continued iterations, the 1-MeHa$_2$PbI$_4$ data show the emergence of new cold crystallization peaks at higher temperatures (guided by two red dotted lines), which subsequently exhibit melting at a lower temperature (~140°C, indicated by red dashed line for the melting endotherm) representing the formation of a secondary phase. The conversion is completed at the 90th iteration. The dotted arrow in* ***a****) shows the glass transition regime. The vertical axis is only for representation of scale of magnitude, i.e., the curves are vertically offset for clarity.*

Impact of thermal cycling on structure and phase stability: Beyond making vitrification more favorable upon multiple heat-cool cycles, we also observed a minor and gradual reduction in the peak melting temperature (T_m) (inset of Figure 1b) on performing multiple heat-cool cycles. Conventional DSC measurements performed at various heat-cool ramp rates over multiple iterations show a similar trend—i.e., reduction in melting and crystallization temperatures during the heating and cooling processes, respectively (Figure S2). We hypothesize that extended exposure at elevated temperature leads to partial loss of organic components and HI, resulting in a reduction of the number density of hydrogen bonds in the perovskite moiety. Reduction in number of hydrogen bonds may in turn induce a gradual decrease in the melting and crystallization temperatures.[9]

Additionally, the conventional DSC performed on 1-MeHa$_2$PbI$_4$ shows two solid-solid structural transitions, T_{s1} at ~100 °C and T_{S2} at ~160 °C prior to the melting transition (Figure S2).[19] However, iterative measurements carried out at varied heating rates (2, 20, and 50 °C/s) show the partial quenching of T_{s1} and T_{S2} at higher ramp rates after the initial heating cycle, pointing to the sluggish kinetics of these structural transitions (Figure S2). The sluggish behavior in turn is reflected in the flash-DSC heating and cooling curves, wherein structural transition peaks do not appear during the faster ramp rate measurements (Figure 1b). In addition, on performing temperature dependent in-situ XRD on a thin-film sample (Figure S6a), we observe a discontinuous shift in the primary diffraction peak from $2\theta = 5.2°$, a characteristic of the room temperature phase (below T_{s1}), to $2\theta = 5.0°$, a characteristic of the high temperature phase (above T_{s1}).[19] However, upon cooling the sample back to room temperature (below T_{s1}), only partial recovery of the room temperature phase ($2\theta = 5.2°$) is observed, further confirming the sluggish transformation kinetics and the dominance of the high temperature phase (which exist above T_{s1}) even at room temperature, after thermal cycling.

Organic and HI loss at elevated temperature can also ultimately result in the generation of a new unidentified phase, which was tracked through flash-DSC as well as in-situ and ex-situ XRD measurements. Though the cooling curves obtained after complete melt quenching (post 31st iteration) did not change substantially, there was significant change observed in the heating curves over the course of 90 iterations (Figure 2b). Characteristics of the parent phase 1-MeHa$_2$PbI$_4$ with T_p ~45 °C and T_m ~158 °C were seen during the 31st heating cycle in Figure 2b (guided by green dotted and dashed lines, respectively); however, with continued iterations, a new unidentified phase starts to emerge, leading to multiple competing exotherms and endotherms. The complete conversion to this unidentified phase occurs at the 90th iteration with T_p ~ 88 °C, and T_m ~140 °C (guided by red dotted and dashed lines, respectively in Figure 2b). The emergence of the two new exotherms (indicated by red dotted lines in Figure 2b) during the intermediate iterations (after the 31st and before the 90th iteration) is unlikely to be attributed to any new polymorphic structural transitions, due to the absence of enthalpy recovery in subsequent cooling runs, which is typically observed for structural transitions (a representative example is provided in Figure S2). Rather, we attribute these peaks to cold crystallization of the new phase(s).

The conversion of 1-MeHa$_2$PbI$_4$ to another stoichiometric phase (distinct T_m ~140 °C) is also tracked using XRD measurements through prolonged heating of a 1-MeHa$_2$PbI$_4$ film, which shows

the emergence of a new peak at $2\theta = 5.6°$ (Figure S6b).[35] The appearance of the film also changes from clear yellow to translucent yellowish white on prolonged heating (Figure S7). We hypothesize that the partial decomposition (organic/HI loss) leads to the generation of this new structurally relaxed phase. Loss of organic and HI was also evident from the flash-DSC measurement in the form of a white halo formed on the UFS-1 chip (Figure S8) due to degradation-induced (during temperature hold at 180 °C) organic amine/organic salt condensation during the fast-cooling runs (programmed from 180° C to -100 °C). Thermogravimetric analysis (TGA) of 1-$MeHa_2PbI_4$ further supports the hypothesis of organic and HI loss, which suggests that, even though the bulk degradation onset temperature (T_d) is 204 °C, a significant amount of decomposition (2% organic loss with respect to the hybrid) occurs at temperatures as low as 180 °C (Figure S9).

To provide an upper limit estimate on organic and HI loss (or compositional change) needed to facilitate glass formation under the employed cooling rate (6000 °C/s), we made use of combustion (C-H-N) and energy-dispersive X-ray spectroscopy (EDXS) techniques to find the relative percentages of individual elements (C, H, N, Pb, and I) across different types of 1-$MeHa_2PbI_4$ samples. Three types of samples were prepared, namely pristine 1-$MeHa_2PbI_4$ crystals (Sample A), spin-coated thick-film before significant organic/HI loss (Sample B, Figure S10), and a spin-coated thick-film after sufficient organic/HI loss to show the beginning of new phase formation (diffraction peak at $2\theta = 5.6°$ clearly observed) (Sample C, Figure S10). Preparation details of the samples are provided in the Methods section. C-H-N and EDXS analyses (Table 1; Figure S11) for sample A show near expected composition relative to the theoretical stoichiometric values for all the elements. However, sample B shows slightly reduced H and I (~3-4%) content, perhaps suggesting some partial (inadvertent) loss of HI due to extended annealing of the thicker films to remove the DMF solvent (see Methods). Sample C shows a significantly higher value (~14%) of C and N loss. Correspondingly, the loss of hydrogen is found to be ~24%, in agreement with the loss of iodine (~23%) obtained through EDXS measurement (Figure S11; Table 1), suggesting HI as the major degradation product. Computation of molar mass value from Table 1 for sample C points to a 15.8% reduction in mass, indicating a threshold of maximum overall mass loss that initiates the formation of the new unidentified phase (T_m ~140 °C). However, the obtained estimate should be considered an upper limit for the formation of the new phase (given the challenge of deconvolving X-ray peaks during the sample preparations process). The formation of the glass in the pristine phase, which occurs before the new phase formation (as shown in Figure S12), is expected to occur at a lower mass loss value. The increased propensity towards glass formation after a certain degree of mass loss has also been recently reported in metal-organic frameworks and organic ligand (non-halide) based perovskites, and is thought to arise from substantial ligand decomposition.[36, 37] The mechanism that results in the hindered reorganization of a melt into a crystalline structure after mass loss remains unclear and a topic of interest for future study.

Table 1. *Combustion analysis of the constituent elements namely, carbon, hydrogen, and nitrogen (C-H-N) obtained for the pristine 1-$MeHa_2PbI_4$ crystals (Sample A), scratched thick film prior to substantial organic/HI loss (Sample B), and after organic/HI loss (Sample C). EDXS analysis of I/Pb ratio was also performed on the respective samples over a large substrate area. The values shown denote the percentage relative to the expected values calculated from the ideal*

*stoichiometry of 1-MeHa$_2$PbI$_4$. The slight deviations in the C and N for samples A and B from the theoretical 100% lie within the uncertainty of the measurement. However, the ~4% loss of HI (inadvertent) for Sample B may be ascribed to the extended annealing of the thick film to remove DMF. *The number in the parenthesis is the standard deviation (SD) and is computed from 2 sets of measurements.*

Elements	Sample A % (SD)	Sample B % (SD)	Sample C % (SD)
C	99.74 (0.01)	100.89 (0.16)	85.54 (0.05)
H	99.35 (0.01)	96.74 (0.01)	75.85 (0.05)
N	101.45 (0.00)	100.27 (0.04)	87.76 (0.04)
I (EDXS)	98.75	95.75	77.00

Kinetics of glass crystallization: After elucidating the role of organic and HI loss in stabilizing the glass phase in organic-deficient 1-MeHa$_2$PbI$_4$, the underlying kinetics of the glass-crystal transformation has been studied to gain a better understanding of the crystallization behavior across a range of temperature (T_g - T_m). The kinetic study requires ensuring protection against further organic/HI loss during the measurement to restrict the emergence of the unidentified phase (with T_m ~ 140 °C). Hence, upon forming a melt quenched glass of the slightly off-stoichiometric 1-MeHa$_2$PbI$_4$ (after 16 heat-cool iterations using the highest achievable cooling rate of 6000 °C/s, Figure 1a), a tiny volume of silicone oil is applied to cover the sample on top of the heater region of the UFS-1 chip (i.e., the silicone oil forms a physical barrier to further organic/HI loss). After this step, the sample was subjected to a series of heat-cool cycles employing a range of heating rates (coarse distribution: 100 °C/s – 10,000 °C/s (Figure 3a) and fine distribution: 100 °C/s- 1000 °C/s (Figure S13)) while maintaining the same cooling rate of 6000 °C/s. With increased heating rate, T_p is seen to shift to higher temperatures whereas T_m remains relatively constant. The shift of ΔT_p = 52 °C over the two orders of employed heating rates provides an ample temperature window to study glass crystallization behavior. The constancy of T_m (thermodynamic characteristic) over all the heating rates suggests a low degree of temperature lag in the measurements (Figure S14). For comparison, an empty chip doesn't show any exotherms or endotherms across the heating ramp range of 100 - 10,000 °C/s employed in the measurement (Figure S15). When the curves obtained at a heating rate of 250 °C/s are compared, no differences are observed between the curves with silicone oil (Figure 3a) and without silicone oil (Figure 1b), highlighting that the oil does not impact the measured features. Furthermore, upon repeating the first cycles (250 °C/s and 100 °C/s for coarse and fine measurement runs, respectively) at the end of the measurement, the positions of T_p and T_m remain the same as for the initial run, revealing the robust nature (minimized organic/HI loss) of the measurement obtained under silicone oil (Figure S16).

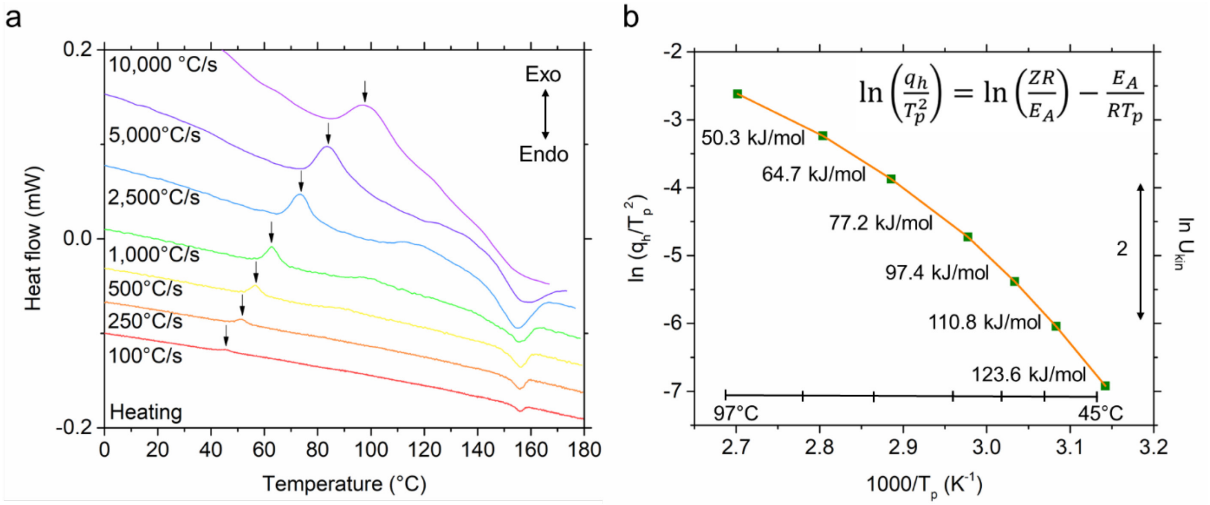

Figure 3. a) *The underlying kinetic effect of glass crystallization in organic-deficient 1-MeHa₂PbI₄ perovskite. With increase in heating ramp rates, a gradual shift in the cold crystallization peak is observed whereas the melting endothermic peak remains constant. The arrow indicates the peak position of cold crystallization (T_p) of the glassy state.* ***b)*** *The shifts in T_p values are used in constructing a Kissinger plot to determine the activation energy of glass crystallization (E_A, slope of the curve) in 1-MeHa₂PbI₄. The slope of the plot shows large deviation from a linear trend over the course of change in heating ramp rates (100°C/s - 10,000°C/s) revealing breakdown of Arrhenius behavior (typical of a fragile liquid).*[26]

Given the T_p values obtained from the various heating curves (100-10,000 °C/s, from Figure 3a & Figure S14a), we can use them to obtain the activation energies of glass crystallization by employing the well-celebrated Kissinger model. The Kissinger model is a non-isothermal extension of Arrhenius and first-order reaction rate equations, that provides the activation energy (E_A) corresponding to the crystallization fraction with the highest crystallization rate, i.e., it considers the change in the peak position of the crystallization exotherm (T_p) as a function of heating rate (q_h).[38] The simplicity of the model facilitates the extraction of activation energy (E_A) from the slope of equation (i),

$$\ln\left(\frac{q_h}{T_p^2}\right) = \ln\left(\frac{ZR}{E_A}\right) - \frac{E_A}{RT_p} \qquad \text{(i)}$$

where R is the gas constant and Z is a pre-exponential factor from the Arrhenius equation. In conventional DSC measurements, the q_h range is narrow, and hence the Kissinger plots tend to yield a straight line and a single E_A value.[9, 39] However, when the employed q_h can be extended (such as in flash-DSC measurements), the plot may also be nonlinear, thereby showing breakdown of Arrhenian behavior. Such reduction in E_A at higher temperatures, as seen for 1-MeHa₂PbI₄ (Figure 3b), is a characteristic of a fragile glass former, as opposed to a single-valued E_A (straight line) characterizing a strong glass former.[26, 28] The activation energy reduces from 124 kJ/mol to 50 kJ/mol when the glass is kinetically forced to crystallize at 45 °C to 97 °C, respectively. In contrast, in our earlier report, the Kissinger plot obtained for another exemplary MHP glass former,

SNPB, yielded a single activation energy of 365 kJ/mol at a similar energy landscape (~110 °C).[9] The lower value of activation energy in 1-MeHa$_2$PbI$_4$ corroborates the faster crystallization kinetics when compared to SNPB.[9] The 1-MeHa$_2$PbI$_4$ melt also shows ~2 order of magnitude smaller viscosity when compared to SNPB (Figure 4) over a range of temperatures above T_m. The bulky and rigid organic spacer (S-(−)-1-(1-naphthyl)ethyl-ammonium) in SNPB presumably imparts more resistance to molecular movement in the melt state, thereby frustrating the ordering kinetics and leading to stronger glass forming ability.[1, 40] In contrast, the more flexible 1-methylhexylammonium cation in 1-MeHa$_2$PbI$_4$ leads to lower viscosity and faster crystallization kinetics. Furthermore, the Turnbull criterium[8] (T_g/T_m) of 1-MeHa$_2$PbI$_4$ is calculated as 0.66, which is smaller than for SNPB ($T_g/T_m \approx 0.76$), further reflecting the requirement of higher cooling rate to vitrify the former.

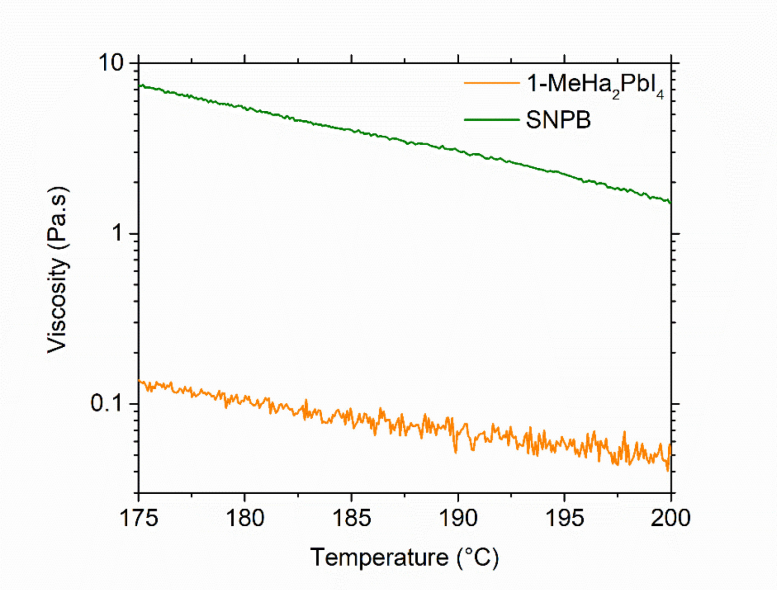

Figure 4. *The melt viscosity values of SNPB (good glass former) vs 1-MeHa$_2$PbI$_4$ (poor glass former) as a function of temperature during the cooling run. The viscosity of the SNPB melt is high enough (compared to the latter) to frustrate molecular reorganization during cooling, giving rise to significantly different glass-crystal switching speeds. The cooling and shear rates employed for the viscosity measurement are 10 °C/min and 10 s^{-1}, respectively.*

To study the crystallization kinetics, we employed a combination of kinetic, thermodynamic, and rheological modelling, which helped in the construction of the Angell plot determination of the fragility index, and the crystal growth rate of 1-MeHa$_2$PbI$_4$. To do so, we fitted the T_p values (Kissinger plot) to a set of rheological and kinetic expressions (explained later in the text) to describe the temperature dependence of crystal growth according to the procedure mentioned in the literature[27, 28] under a set of assumptions. The foremost criterion is the validity of the Kissinger method to study the crystal growth rates under non-isothermal measurement conditions. We know that the activation energy obtained from the Kissinger method is generally that of crystal growth,[41] which holds true for a growth dominant crystallization mechanism. However, for a nucleation

dominant crystallization mechanism, there could be a possibility of some overlap between nucleation and growth processes during the non-isothermal DSC measurements. Nevertheless, the overall crystallization process is a weighted average of the contribution from nucleation and growth processes, wherein the contribution of the former is significantly less at the later stages of crystallization (near T_p) and thus can be ignored.[26] Furthermore, our recently reported work on crystallization kinetics of SNPB shows an Avrami parameter (n) of 2, suggesting crystallization proceeds through nucleation site saturation, which is subsequently followed by 2-dimensional crystal growth (corroborated using in-situ and ex-situ microscopy).[9] Owing to the similarity in the molecular and morphological dimensions of crystalline SNPB and 1-$MeHa_2PbI_4$, we assume that the contribution of nucleation at the later stages of crystallization is minimal and can be ignored, thus supporting the fact that the activation energy given by Kissinger method is of crystal growth. The second requirement is that Johnson-Mehl-Avrami (JMA) crystallization kinetics can be applied under non-isothermal conditions only when the crystal growth rate is constant i.e., it depends only on temperature and not time.[9, 42] This requirement can generally be fulfilled if the transformation from the glassy to crystalline state does not involve a change in composition. In our MHP system, the transformation from the glassy to crystalline state does not involve a change in composition, and only results in a single-phase perovskite (which was ensured by preventing the formation of unwanted phases using silicone oil during the measurement). Therefore, we can use our data to construct a Kissinger plot and study the temperature dependence of the kinetic coefficient for crystal growth.

The plot of $\ln(q_h/T_p^2)$ vs $1/T_p$ provides a curve with a slope of E_A for crystal growth at any temperature. Thus, the obtained values from the Kissinger plot would match the gradient of crystal growth with temperature i.e., the slope of $\ln(U_{kin})$ vs $1/T$.[42] Hence, the data points depicted in Figure 3b can be considered to fit a relative kinetic component of crystal growth U_{kin} (m/s),[27, 28, 42-45] which when combined with a thermodynamic model provides crystal growth rate U (m/s) as a function of temperature[46] given by (ii),

$$U = U_{kin}\left[1 - exp\left(-\frac{\Delta G}{RT}\right)\right] \qquad \text{(ii)}$$

where R is the gas constant as mentioned above, and ΔG (kJ/mol) is the crystallization driving force, which can be reasonably expressed for a fragile glass former as suggested by Thompson and Spaepen,[26, 47] as (iii)

$$\Delta G = \frac{\Delta H_m \Delta T}{T_m}\left(\frac{2T}{T_m + T}\right) \qquad \text{(iii)}$$

where ΔH_m (kJ/mol) is the melting enthalpy, T_m (K) is melting temperature, and ΔT (= $T_m - T$) is the undercooling temperature.

However, to extrapolate the crystal growth rate, the U_{kin} should be fit with an appropriate model that can be associated with a physically measurable quantity such as viscosity. The Stokes−Einstein equation[47] establishes such a relation between U_{kin} and viscosity η (Pas), yielding $U_{kin} \propto \eta^{-1}$, and expressed by (iv)

$$\log_{10}\eta = C - \log_{10} U_{kin} \qquad \text{(iv)}$$

where C is a constant, reflecting the difference between viscosity and reciprocal of U_{kin}, which can be obtained from adjusting viscosity at T_m (η_{Tm}).[28, 42] Hence, the reciprocal of relative U_{kin} can first be fitted on the Angell plot using the viscosity expression by taking $C = 0$ in (iv). Herein we use the widely employed viscosity-temperature model presented by Mauro, Yue, Ellison, Gupta, and Allan (MYEGA)[48] given in expression (v),

$$\log_{10}\eta = \log_{10}\eta_\infty + (12 - \log_{10}\eta_\infty)\frac{T_g}{T} \times exp\left[\left(\frac{m}{12-\log_{10}\eta_\infty}\right)\left(\frac{T_g}{T} - 1\right)\right] \qquad \text{(v)}$$

where $\log_{10}\eta_\infty$ is the viscosity at infinite temperature (obtained from intercept with y-axis), T_g is the glass transition temperature, and m is the fragility index. The MYEGA model has proven to be an excellent choice to extrapolate the viscosity values of a non-Arhenian liquid to either ends of the temperature range, and is considered to provide a superior fit[43, 48] relative to predecessor approaches such as Vogel–Fulcher–Tammann (VFT),[49] Avramov–Milchev (AM),[50] and Cohen-Grest (CG)[51] viscosity models, while having the fewest number of fitting parameters.

Hence, considering T_g = 15.5°C, the inverse of U_{kin} (i.e., U_{kin}^{-1}) is modeled using the MYEGA expression (v) to yield an Angell plot. However, the modeled viscosity curve doesn't overlap with the experimental viscosity value above T_m, suggesting the requirement of translation along vertical axis (i.e., $C \neq 0$) to convert the relative U_{kin} to absolute U_{kin} (Figure 5). Additionally, the model produces a viscosity nearly 5.5 orders of magnitude lower than anticipated $\eta = 10^{12}$ Pa.s at T_g [48, 52] hinting toward breakdown of the Stokes−Einstein relation. This necessitates the employment of Ediger's decoupling coefficient to account for the mismatch.[46] Ediger proposed that the Stokes-Einstein relation usually breaks below T_m in a fragile supercooled liquid (such as the present system) and thus the model needs be modified using the relation, $U_{kin} \propto \eta^{-\xi}$, which can be expressed by (vi) (modified version of (iv)),

$$\log_{10}\eta = C' - \xi \,.\log_{10} U_{kin} \qquad \text{(vi)}$$

where ξ is the decoupling coefficient and C' is the displacement required in the vertical axis to match the experimentally measured viscosity. Using a value of $\xi = 0.40$, the viscosity at T_g can be matched with 10^{12} Pa.s and, using a value of $C' = 0.80$, the modelled viscosity can be matched with the experimental viscosity value, resulting in an Angell plot with the fragility index of m = 72 and $\log_{10}\eta_\infty$ = -3.72 (Figure 5).

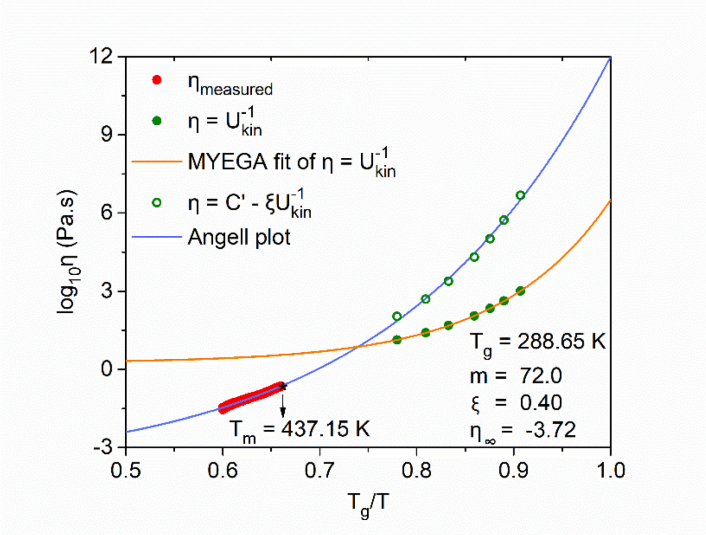

Figure 5. *Angell plot showing the viscosity-temperature dependence. The inverse of the MYEGA fitted relative U_{kin} (i.e., U_{kin}^{-1}) obtained using equation (iv) and (v) with C=0, yields a viscosity plot (filled green dots, orange curve). However, a reduced viscosity value by 5-6 order of magnitude at the measured glass transition temperature (T_g), relative to the expected viscosity value of 10^{12} Pa.s at T_g,[48, 52] highlights a breakdown of the Stokes-Einstein relationship at lower temperatures.[53] Hence, constructing a plot of U_{kin}^{-1} on applying a decoupling coefficient of ξ = 0.40 and a translational constant of C' = 0.80, (open green dots, using equation (v) and (vi)) leads to an actual Angell plot (blue curve) that overlaps with measured viscosity values (red dots) and the anticipated viscosity value of 10^{12} Pa.s at T_g, with a fragility index of m = 72.*

The extracted value of fragility index is higher than SNPB ($m \approx 42$), showing the higher fragility and thus the requirement of higher cooling rate to access the glassy state.[9] After finding the viscosity-temperature dependence, equation (vi) can then be used to obtain the temperature dependence of absolute U_{kin} (Figure 6a). Hence, using the equation (ii) and (iii), ΔH_m (6.63 kJ/mol, obtained through conventional DSC, see Methods), T_m (437 K), and the obtained absolute U_{kin}, the overall crystal growth (U) across a wide temperature range (T_g to T_m) can be extrapolated (Figure 6b). The maximum crystal growth rate (U_{max}) occurs at $0.93T_m$ with a value of 0.21 m/s. This suggests possible applicability of 1-MeHa$_2$PbI$_4$ or related systems in phase change applications with moderate switching speed of ~100Mbits/s for nanoscopic devices. The switching is expected to be even faster if the melt can be vitrified at higher cooling rates (>6000 °C/s; beyond the capability of the current flash-DSC experiment) without relying on slight loss of organic components to access the glassy state. Having control over melt quench rates will likely push the switching speed by orders of magnitude higher than the currently extracted value. Furthermore, given the essentially unlimited possibility to tune the chemical components (organic/inorganic) of hybrid MHPs, it is expected that glass-crystalline transition properties can be further tuned for a variety of prospective applications.

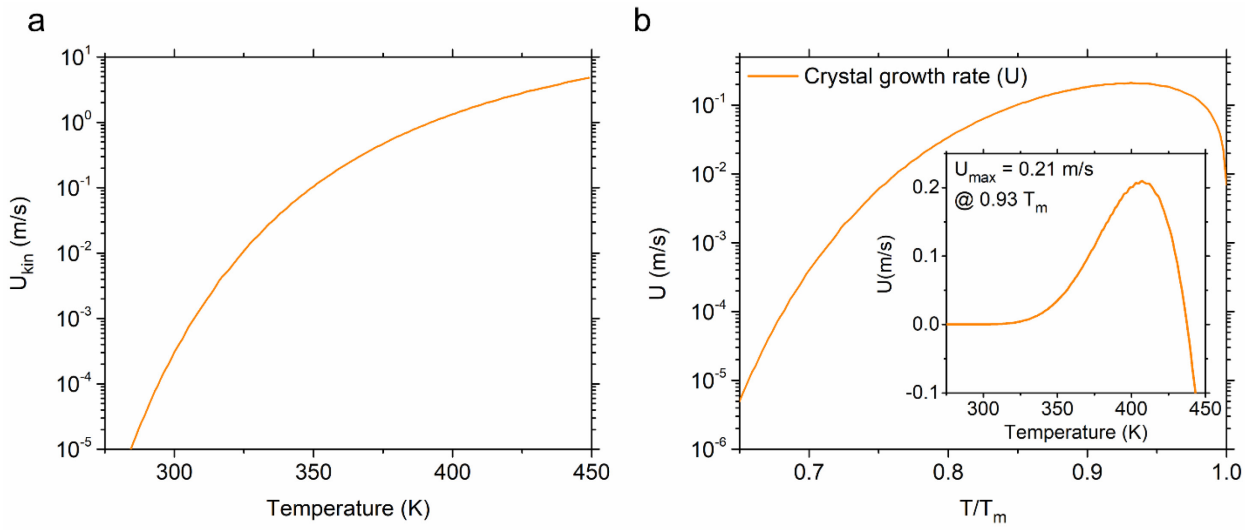

Figure 6. a) *Temperature dependence of the absolute kinetic component of crystal growth rate (U_{kin}) obtained from equation (vi).* ***b)*** *The overall crystal growth rate obtained from the combination of kinetic and thermodynamic contributions. The maximum crystal growth rate is extracted to be 0.21 m/s at ~0.93T_m, as obtained from the linear scale plot in the inset.*

Conclusion

In summary, for the first time we demonstrate glass formation in a 2D hybrid lead iodide perovskite, 1-MeHa$_2$PbI$_4$, using ultrafast calorimetry. The presence of the relatively flexible organic spacer, 1-methyl-hexylammonium, unlike the previously demonstrated more rigid S-(-)-1-(1-naphthyl)ethylammonium cation, imparts faster ordering kinetics, hence requiring cooling rates in excess of 6000 °C/s to produce a melt quenched glass. Slight loss of organic and HI at elevated temperatures reduces T_m and helps frustrate melt reordering and allows access to a glassy state with T_g ~ 16 °C in the exemplary perovskite. Kissinger modelling and the iterative calorimetric experiments performed over two orders of heating rate (100 – 10,000 °C/s) enable the extraction of activation energies of crystallization (E_A) across a wide temperature range (45 – 97 °C). A reduction in E_A from 124 to 50 kJ/mol with increasing temperature reveals the fragile nature of the glass, which is probed through a combination of kinetic, thermodynamic, and rheological modelling to yield the fragility index and crystal growth rate. Furthermore, we report the measurement of MHP melt viscosity, comparing a good (SNPB) with a poor (1-MeHa$_2$PbI$_4$) glass former. This measurement helps corroborate the disparate ordering kinetics between the two types of glass-forming MHPs. The extracted crystal growth rate of 0.21 m/s for 1-MeHa$_2$PbI$_4$ offers some promise for application in prospective devices requiring fast switching (although the low glass transition temperature implies that the glass state will be unstable at room temperature). Given the wide compositional space for MHP tunability and the broad range of ramp rates supported by ultrafast calorimetry, it is conceivable to diversify the family of glass forming MHPs and to create a stable glassy state at room temperature while also allowing for fast crystallization at elevated temperatures, with contrasting optoelectronic character in either state for practical applications in, e.g., metamaterials, nonvolatile memory, and optical and neuromorphic computing devices.

Experimental Section

Materials. (S)-(−)-1-(1-naphthyl)ethylamine (>99%, Sigma Aldrich), 2-aminoheptane (1-methylhexylamine, 99%, Sigma Aldrich), lead bromide ($PbBr_2$, 99.99%, TCI Chemicals), lead iodide (PbI_2, 99.99%, TCI Chemicals), hydroiodic acid (HI) solution (57 wt% in H_2O, stabilized, 99.95%, Sigma Aldrich), and hydrobromic acid (HBr) (48 wt% in H_2O, >99.99%, Sigma Aldrich) were procured and used without further purification.

Crystal synthesis. Crystals of $(1\text{-MeHa})_2PbI_4$ (1-MeHa = 1-methyl-hexylammonium) were prepared by mixing stoichiometric amounts of PbI_2 (55.3 mg, 0.12 mmol) and 2-aminoheptane (36.1 μL, 0.24 mmol) in HI (1 mL) solution in a sealed vial at 95 °C. The hot solution was then slowly cooled to room temperature (20 °C) over a period of 24 h in a water bath, resulting in the formation of yellowish $(1\text{-MeHa})_2PbI_4$ perovskite crystals. The crystals were cleaned and washed with diethyl ether and stored in N_2 glove box.

To grow *S*-NPB perovskite crystals, stoichiometric amounts of $PbBr_2$ (90 mg, 0.24 mmol) and (*S*)-(−)-1-(1-naphthyl)ethylamine (78 μL, 0.48 mmol) were dissolved in aq. HBr (1.0 mL) and deionized water (2.4 mL) in a sealed vial at 95 °C. The hot solution was slowly cooled to room temperature (21 °C) over a period of 24 h in a water bath, resulting in the formation of colorless plate-like *S*-NPB single crystals. The crystals were cleaned and washed with diethyl ether and stored in a N_2 glove box.

Solution processing of thin films. Soda-lime glass substrates (10.0 × 10.0 × 1.2 mm^3) were cleaned by ultrasonication in acetone, isopropyl alcohol and deionized water for 10 min each. Upon air drying the substrates, they were subjected to Ar–O_2 plasma treatment for 10 min. A solution (0.2 M) of $(1\text{-MeHa})_2PbI_4$ perovskite crystals in DMF was spin-coated on pre-cleaned soda-lime glass substrates at a spin speed of 3000 rpm for 30 s inside a N_2-filled glovebox and then subjected to a 10-minute anneal at 100 °C.

X-ray diffraction study. The X-ray diffraction (XRD) measurements of bare crystals and thin films were performed on a PANalytical Empyrean powder X-ray diffractometer using Cu Kα radiation, with the X-ray tube operating at 45 kV and 40 mA. *Ex-situ* measurements were carried out over the 2θ range of 3° to 50° for the phase characterization.

For the *in-situ* phase change test (emergence of new phase due to loss of components), the measurement was conducted over the 2θ range of 3° to 30° on a PANalytical Empyrean X-ray diffractometer using Cu-Kα radiation with HTK-1200N temperature stage under nitrogen flow. The thin film samples were ramped from room temperature to 100 °C, isothermally held at 100 °C for 4 hours and then brought back to room temperature (Figure S6).

Conventional calorimetry. DSC measurements were performed using a TA Discovery DSC instrument using a hermetically sealed aluminum pan and lid. Prior to experiments, the DSC setup was calibrated with metallic indium (melting temperature: 156.6 °C; enthalpy of melting: 28.71 J g^{-1}), which upon repeating the experiment showed an acceptable temperature offset of 0.2 °C and melting enthalpy offset of 0.04%. Calibration and the above measurement were carried out at a ramp rate of 5 °C/min. After hermetic sealing, the three pans with 1-MeHa_2PbI_4 crystals (~5 mg each) were exposed to a heating cycle with ramp rates of 2, 20, and 50 °C/min, respectively, over

a temperature range of 25 to 185 °C and held isothermally at 185 °C for 10 seconds, before cooling back to room temperature at the same ramp rates. The same process was iterated two more times to observe the effects of thermal cycling (Figure S2). The enthalpy of melting/crystallization (ΔH_m) was obtained through the area under the crystallization exotherm, which was determined to be approximately 6.63 kJ/mol for 1-MeHa$_2$PbI$_4$.

Ultrafast calorimetry. Ultrafast ("flash") DSC measurement was performed using the flash-DSC1 instrument (with UFS-1 chip-sensor), henceforth called flash-DSC, manufactured by Mettler Toledo. The technical specification of the instrument suggests that cooling rates of up to 4,000 °C/s are supported in the temperature range of -100 °C – 450 °C. Programming a higher cooling rate (>4000 °C/s) is possible; however this approach results in loss of information at lower temperatures due to undershoots and the sudden drive to equilibrate at the end temperatures.[21] Since our region of interest (crystallization or glass formation during cooling) is in the higher temperature regimes, we thereby employed 6,000 °C/s for much of the current study. The UFS-1 chip sensor was mounted into the flash-DSC instrument and was conditioned and corrected over the temperature range of 173K (-100 °C) to 723K (450 °C) to release any inbuilt stress. The N_2 flow was maintained at 35 ml/min throughout the series of experiments. After this step, the as-prepared crystals of 1-MeHa$_2$PbI$_4$ were poured on a glass slide and a small single crystal flake (~100 ng) was isolated under an optical microscope and affixed to the flash-DSC chip-sensor. To mount the crystal, a hair isolated from a hairbrush was used to electrostatically select the crystal from the glass slide and transfer it to the central active region of the UFS-1 chip (Figure S4). To establish thermal contact between the crystal and the chip (by an initial melting sequence), the instrument was provided with an initial parameter set to ramp from room temperature (~25 °C) to 180 °C at 10,000 °C/s with subsequent isothermal hold of 1.5 seconds. After this, for the initial flash-DSC iterative study (as in Figure 1), the instrument was programmed to iterate between -100 °C and 180 °C with the following steps: 1. Cool from 180 °C to -100 °C at 6000 °C/s; 2. Isothermal hold (dwell) at -100 °C for 1 second; 3. Heat from -100 °C to 180 °C at 250 °C/s; 4. Isothermal hold (dwell) at 180 °C for 1 second. Repeat steps (1) – (4) for 16 cycles before cooling back to room temperature (25 °C). After observing melt-quenching in the cooling cycle and cold crystallization in the heating cycle, the instrument was programmed to perform a kinetic study after protecting the 1-MeHa$_2$PbI$_4$ sample from further organic loss (Figure 3). To circumvent the organic loss, a tiny volume of silicone oil (type 47V, 60000, purchased from Silitech AG and recommended to be used in flash-DSC up to 350 °C)[54] was applied to the central active region of the UFS-1 chip to submerge the 1-MeHa$_2$PbI$_4$ sample, using a hair isolated from a hairbrush. Flash-DSC measurements with and without oil don't lead to any additional feature or significant differences in the measurements within the temperature range of interest (-100 °C – 180 °C).

For the coarse kinetics study, (Figure 3a), the instrument was programmed to reach 180 °C from 25 °C at 10,000 °C/s and isothermally held at 180 °C for 1.5 seconds. After this sequence, the instrument sequence was appended with the following iterative steps: 1. Cool from 180 °C to -100 °C at 6000 °C/s; 2. Isothermal hold (dwell) at -100 °C for 1 second; 3. Heat from -100 °C to 180 °C at x °C/s; where x = 100, 250, 500, 1000, 2500, 5000 and 10000 °C/s, respectively; 4. Isothermal hold (dwell) at 180 °C for 1 second. Steps (1) – (4) were repeated with different x values in step (3). To examine if there was any change incurred due to thermal cycling under silicone oil, another iteration with heating rate of 250 °C/s was performed, which appeared to match the initial 250 °C/s run, thereby confirming the role of silicone oil in protecting the sample from organic loss (Figure S16a). For the finer kinetic study, the instrument was programmed as explained above except for

changing the *x* values in step (3) to 100, 200, 300, 400, 500, 600, 700, 800, 900 and 1000 °C/s. To examine if there was any change incurred due to thermal cycling under silicone oil, another iteration with heating rate of 100 °C/s was performed, which led to results that appear to match the initial 100 °C/s run, thereby further confirming the effective role of silicone oil in protecting the sample from organic loss (Figure S16b).

To study the glass transition and the emergence of the unidentified phase (Figure 2), a lower cooling rate of 3000 °C/s (compared to the previously used 6000 °C/s) is employed to extend the range of measurement to lower temperatures, which helped extract information on the glass transition over multiple heat-cool cycles. Hence, the instrument was programmed to iterate between -100 °C and 180 °C with the following steps: 1. Cool from 180 °C to -100 °C at 3000 °C/s; 2. Isothermal hold (dwell) at -100 °C for 1 second; 3. Heat from -100 °C to 180 °C at 250 °C/s; 4. Isothermal hold (dwell) at 180 °C for 1 second. Repeat steps (1) – (4) for 90 cycles before cooling back to room temperature (25 °C).

To demonstrate reusability of the UFS-1 chip sensor, the chip containing a previously cycled 1-$MeHa_2PbI_4$ sample was successively washed with DMF, acetone, and iso-propanol and left to dry in ambient. It was then mounted into the flash-DSC instrument, wherein it was conditioned and corrected over the temperature range of 173K (-100 °C) to 723K (450 °C) to release any inbuilt stress. Another small single crystal flake was loaded on it to perform similar measurements (Figure S17) showing repeatability as well as reusability of the UFS-1 chip. Despite the reusability of the UFS-1 chip sensor, all measurements in the current study used new chips for each separate measurement. In this sense, the primary reason for displaying the ability to clean and reuse the sensor is to demonstrate that the perovskite melt does not react or adversely interact with the materials comprising the chip during the measurement.

Viscosity measurements. The viscosity of the two perovskite (SNPB and 1-$MeHa_2PbI_4$) samples were measured using a TA Discovery HR30 rheological tool under nitrogen purge with 8.00 mm parallel plate configuration. The samples were finely powdered and pressed into a small disc and loaded onto a preheated lower plate at 200 °C. After lowering the upper plate, it was verified that the liquefied melt completely filled the space between plates (gap ~ 0.42 mm). After that, the temperature was lowered at a rate of 5 °C/min and instantaneous viscosity values were recorded at each temperature (Figure 4). The melting point (T_m = 164 °C) was measured as the onset of crystallization while cooling the melt, which was also corroborated with the DSC measurements in Figure S2.

Mass loss analysis using EDXS and C-H-N measurement. Energy-dispersive X-ray spectroscopy (EDXS) and combustion analysis were performed to extract the relative percentages of the constituent elements (C, H, N, Pb, and I) across different types of 1-$MeHa_2PbI_4$ samples. We prepared three forms of samples, namely, pristine 1-$MeHa_2PbI_4$ crystals (Sample A), spin-coated thick-film before any intentional organic/HI loss (Sample B), and a spin-coated thick-film after some organic/HI loss (due to heating) that shows the beginning of new phase formation (from X-ray diffraction), which diffracts at 2θ = 5.6° (Sample C, Figure S10).

Sample A is prepared using the slow cooling method described in the 'Crystal synthesis' section. Two sets of pristine 1-$MeHa_2PbI_4$ crystals were used for the C-H-N analysis.

Sample B is prepared by spin coating a 0.78M solution of 1-MeHa$_2$PbI$_4$ crystals in DMF at 3000 RPM for 30 seconds to yield thick films. After spin coating, the samples were annealed for 80 minutes at 100 °C in a N_2 filled glove box to remove prospective coordinated DMF. The obtained thick film was then used for the C-H-N analysis after scratching the material off the substrate to obtain two sets of powder (Sample B). The leftover area of the scratched thick film was used to conduct the EDXS measurement to obtain the I/Pb ratio.

Sample C was prepared using the same procedure as followed for Sample B, with additional annealing at 130 °C for 5 hours within a N_2-filled glove box to induce the new phase formation (diffraction peak at $2\theta = 5.6°$) (Figure S10). The obtained thick film was then used for the C-H-N analysis after scratching to obtain two sets of powder (Sample C). The leftover area of the scratched thick film was used to conduct the EDXS measurement to obtain I/Pb ratio.

An Apreo S SEM system by ThermoFisher Scientific was used at 15 kV accelerating voltage for composition analysis over a large area (50x magnification) to obtain EDXS spectra (Figure S11). C-H-N analysis was carried out at Galbraith laboratories using the GLI Procedure ME-14 on two sets of Sample A, B, and C each to obtain reliable statistics (Table 1).

Acknowledgement

This work was supported by the National Science Foundation under Grant No. DMR- 2114117. The work was performed in part at the Duke University Shared Materials Instrumentation Facility (SMIF), a member of the North Carolina Research Triangle Nanotechnology Network (RTNN), which is supported by the National Science Foundation (Grant ECCS-2025064) as part of the National Nanotechnology Coordinated Infrastructure. The flash-DSC work at North Carolina State University (NCSU) was supported by Goodnight Innovation Distinguished Professorship Endowment funds. The authors would like to thank Jenny Forrester from Analytical Instrumentation Facility (AIF), NCSU for helping with the in-situ temperature dependent XRD measurements. The authors would like to thank Yi Xie for training with the crystal growth technique. The authors would also like to thank TA instruments for their help with the temperature dependent viscosity measurements.

Associated contents

Supporting Information

XRD pattern of liquid N_2 melt-quenched film of 1-MeHa$_2$PbI$_4$; Conventional DSC heat-cool cycles of 1-MeHa$_2$PbI$_4$ crystals obtained at various ramping rates; Flash-DSC cooling curves with and without 1-MeHa$_2$PbI$_4$ sample; Photograph of crystal mounted on 1-MeHa$_2$PbI$_4$ UFS-1 chip; Cooling curves with glass transition of 1-MeHa$_2$PbI$_4$ melt obtained at different cooling rates; In-situ temperature dependent XRD pattern of thin spin-coated 1-MeHa$_2$PbI$_4$ film; Photographs of thin 1-MeHa$_2$PbI$_4$ spin coated film before and after organic/HI loss; Photograph of UFS-1 chip with 1-MeHa$_2$PbI$_4$ crystal before and after 90 iterations of heating and cooling; TGA profile of 1-MeHa$_2$PbI$_4$ crystals; Ex-situ XRD profile of thick spin coated film of 1-MeHa$_2$PbI$_4$ at 130 °C for extended duration; EDXS profile of the 1-MeHa$_2$PbI$_4$ crystals and thick spin coated films (before and after organic/HI loss); Trends in T_m over 90 iterations of flash-DSC heat-cool cycles; Flash-DSC heating curves obtained at ramp rate of 100-1000 °C/s; Trends in T_m and T_p of 1-MeHa$_2$PbI$_4$

sample over a range of heating rate (100-10,000 °C/s); Empty run of UFS-1 chip over a range of heating rates (100-10,000 °C/s); Reproducibility test of the flash-DSC measurement; Reusability test of the UFS-1 chip after solvent washing.

References

1. Singh, A.; Jana, M. K.; Mitzi, D. B., Reversible crystal–glass transition in a metal halide perovskite. *Adv. Mater.* **2021,** *33*, 2005868.
2. Singh, A.; Jana, M.; Mitzi, D. B. Organic-inorganic metal halide glass. US Patent Appl. 17/333,862, 2022.
3. Best Research-Cell Efficiency Chart, https://www.nrel.gov/pv/cell-efficiency.html (accessed: May 2023).
4. Jena, A. K.; Kulkarni, A.; Miyasaka, T., Halide perovskite photovoltaics: background, status, and future prospects. *Chem. Rev.* **2019,** *119*, 3036-3103.
5. Min, H.; Lee, D. Y.; Kim, J.; Kim, G.; Lee, K. S.; Kim, J.; Paik, M. J.; Kim, Y. K.; Kim, K. S.; Kim, M. G., Perovskite solar cells with atomically coherent interlayers on SnO2 electrodes. *Nature* **2021,** *598*, 444-450.
6. Chu, Z.; Ye, Q.; Zhao, Y.; Ma, F.; Yin, Z.; Zhang, X.; You, J., Perovskite Light-Emitting Diodes with External Quantum Efficiency Exceeding 22% via Small-Molecule Passivation. *Adv. Mater.* **2021,** *33*, 2007169.
7. Wu, H.; Ge, Y.; Niu, G.; Tang, J., Metal halide perovskites for X-ray detection and imaging. *Matter* **2021,** *4*, 144-163.
8. Turnbull, D., Under what conditions can a glass be formed? *Contemp. Phys.* **1969,** *10*, 473-488.
9. Singh, A.; Mitzi, D. B., Crystallization Kinetics in a Glass-Forming Hybrid Metal Halide Perovskite. *ACS Mater. Lett.* **2022,** *4*, 1840-1847.
10. Saparov, B.; Mitzi, D. B., Organic–inorganic perovskites: structural versatility for functional materials design. *Chem. Rev.* **2016,** *116*, 4558-4596.
11. Mao, L.; Stoumpos, C. C.; Kanatzidis, M. G., Two-dimensional hybrid halide perovskites: principles and promises. *J. Am. Chem. Soc.* **2018,** *141*, 1171-1190.
12. Stern, K.; Wainstein, N.; Keller, Y.; Neumann, C. M.; Pop, E.; Kvatinsky, S.; Yalon, E., Uncovering Phase Change Memory Energy Limits by Sub-Nanosecond Probing of Power Dissipation Dynamics. *Adv. Electron. Mater.* **2021,** *7*, 2100217.
13. Bruns, G.; Merkelbach, P.; Schlockermann, C.; Salinga, M.; Wuttig, M.; Happ, T.; Philipp, J.; Kund, M., Nanosecond switching in GeTe phase change memory cells. *Appl. Phys. Lett.* **2009,** *95*, 043108.
14. Zhang, W.; Mazzarello, R.; Wuttig, M.; Ma, E., Designing crystallization in phase-change materials for universal memory and neuro-inspired computing. *Nat. Rev. Mater.* **2019,** *4*, 150-168.
15. Ielmini, D.; Wong, H.-S. P., In-memory computing with resistive switching devices. *Nat. Electron.* **2018,** *1*, 333-343.
16. Wang, Q.; Rogers, E. T.; Gholipour, B.; Wang, C.-M.; Yuan, G.; Teng, J.; Zheludev, N. I., Optically reconfigurable metasurfaces and photonic devices based on phase change materials. *Nat. Photonics* **2016,** *10*, 60-65.
17. Gong, Z.; Yang, F.; Wang, L.; Chen, R.; Wu, J.; Grigoropoulos, C. P.; Yao, J., Phase change materials in photonic devices. *J. Appl. Phys.* **2021,** *129*, 030902.
18. Slavney, A. H.; Kim, H. K.; Tao, S.; Liu, M.; Billinge, S. J.; Mason, J. A., Liquid and Glass Phases of an Alkylguanidinium Sulfonate Hydrogen-Bonded Organic Framework. *J. Am. Chem. Soc.* **2022,** *144*, 11064-11068.

19. Li, T.; Dunlap-Shohl, W. A.; Reinheimer, E. W.; Le Magueres, P.; Mitzi, D. B., Melting temperature suppression of layered hybrid lead halide perovskites via organic ammonium cation branching. *Chem. Sci.* **2019,** *10*, 1168-1175.
20. Singh, A.; Crace, E.; Xie, Y.; Mitzi, D. B., Two-dimensional lead-free hybrid perovskite semiconductor with reduced melting temperature. *Chem. Commun.* **2023,** *59*, 8302-8305.
21. Mathot, V.; Pyda, M.; Pijpers, T.; Poel, G. V.; Van de Kerkhof, E.; Van Herwaarden, S.; Van Herwaarden, F.; Leenaers, A., The Flash DSC 1, a power compensation twin-type, chip-based fast scanning calorimeter (FSC): First findings on polymers. *Thermochim. Acta* **2011,** *522*, 36-45.
22. Gao, M.; Perepezko, J., Flash DSC determination of the delay time for primary crystallization and minor alloying effect in marginal Al-based metallic glasses. *Thermochim. Acta* **2019,** *677*, 91-98.
23. Gao, M.; Perepezko, J., Separating β relaxation from α relaxation in fragile metallic glasses based on ultrafast flash differential scanning calorimetry. *Phys. Rev. Mater.* **2020,** *4*, 025602.
24. Schick, C.; Mukhametzyanov, T. A.; Solomonov, B. N., Fast Scanning Calorimetry of Organic Materials from Low Molecular Mass Materials to Polymers. *Rev. Adv. Chem.* **2021,** *11*, 1-72.
25. Luo, S.; Li, N.; Zhang, S.; Zhang, C.; Qu, T.; Ocheje, M. U.; Xue, G.; Gu, X.; Rondeau-Gagné, S.; Hu, W., Observation of stepwise ultrafast crystallization kinetics of donor–acceptor conjugated polymers and correlation with field effect mobility. *Chem. Mater.* **2021,** *33*, 1637-1647.
26. Orava, J.; Greer, A. á.; Gholipour, B.; Hewak, D.; Smith, C., Characterization of supercooled liquid Ge2Sb2Te5 and its crystallization by ultrafast-heating calorimetry. *Nat. Mater.* **2012,** *11*, 279-283.
27. Chen, B.; Ten Brink, G. H.; Palasantzas, G.; Kooi, B. J., Crystallization kinetics of GeSbTe phase-change nanoparticles resolved by ultrafast calorimetry. *J. Phys. Chem. C* **2017,** *121*, 8569-8578.
28. Chen, Y.; Wang, R.; Shen, X.; Wang, J.; Xu, T., New methods versus old questions: crystallization kinetics of S, Se, and Te. *Cryst. Growth Des.* **2019,** *19*, 1103-1110.
29. Vermeulen, P. A.; Calon, J.; Ten Brink, G. H.; Kooi, B. J., Combining ultrafast calorimetry and Electron microscopy: reversible phase transformations in SeTeAs alloys. *Cryst. Growth Des.* **2018,** *18*, 3668-3673.
30. Xie, Y.; Song, R.; Singh, A.; Jana, M. K.; Blum, V.; Mitzi, D. B., Kinetically Controlled Structural Transitions in Layered Halide-Based Perovskites: An Approach to Modulate Spin Splitting. *J. Am. Chem. Soc.* **2022,** *144*, 15223-15235.
31. Schawe, J. E. In *Influence of calcium carbonate and carbon nanotubes on the crystallization kinetics of polypropylene at high supercooling*, AIP Conference Proceedings, AIP Publishing LLC: 2016; Vol. 1713, pp 070001. DOI: 10.1063/1.4942287.
32. Moynihan, C. T.; Easteal, A. J.; Wilder, J.; Tucker, J., Dependence of the glass transition temperature on heating and cooling rate. *J. Phys. Chem.* **1974,** *78*, 2673-2677.
33. Parodi, E.; Govaert, L.; Peters, G., Glass transition temperature versus structure of polyamide 6: A flash-DSC study. *Thermochim. Acta* **2017,** *657*, 110-122.
34. Evaluation Possibilities for the Glass Transition, https://www.mt.com/us/en/home/supportive_content/matchar_apps/MatChar_HB401.html (Accessed June 2023).
35. Das, C.; Nishiguchi, T.; Fan, Z.; Horike, S., Crystallization Kinetics of a Liquid-Forming 2D Coordination Polymer. *Nano Lett.* **2022,** *22*, 9372-9379.
36. Shaw, B. K.; Hughes, A. R.; Ducamp, M.; Moss, S.; Debnath, A.; Sapnik, A. F.; Thorne, M. F.; McHugh, L. N.; Pugliese, A.; Keeble, D. S., Melting of hybrid organic–inorganic perovskites. *Nat. Chem.* **2021,** *13*, 778-785.
37. Shaw, B. K.; Castillo-Blas, C.; Thorne, M. F.; Gómez, M. L. R.; Forrest, T.; Lopez, M. D.; Chater, P. A.; McHugh, L. N.; Keen, D. A.; Bennett, T. D., Principles of melting in hybrid organic–inorganic perovskite and polymorphic ABX 3 structures. *Chem. Sci.* **2022,** *13*, 2033-2042.

38. Kissinger, H. E., Variation of peak temperature with heating rate in differential thermal analysis. *J. Res. Natl. Bur. Stand. (U. S.)* **1956,** *57*, 217-221.
39. Blaine, R. L.; Kissinger, H. E., Homer Kissinger and the Kissinger equation. *Thermochim. Acta* **2012,** *540*, 1-6.
40. Jana, M. K.; Song, R.; Liu, H.; Khanal, D. R.; Janke, S. M.; Zhao, R.; Liu, C.; Vardeny, Z. V.; Blum, V.; Mitzi, D. B., Organic-to-inorganic structural chirality transfer in a 2D hybrid perovskite and impact on Rashba-Dresselhaus spin-orbit coupling. *Nat. Commun.* **2020,** *11*, 1-10.
41. Kelton, K. F., Analysis of crystallization kinetics. *Mater. Sci. Eng. A* **1997,** *226*, 142-150.
42. Orava, J.; Greer, A. á.; Gholipour, B.; Hewak, D.; Smith, C., Characterization of supercooled liquid Ge 2 Sb 2 Te 5 and its crystallization by ultrafast-heating calorimetry. *Nat. Mater.* **2012,** *11*, 279-283.
43. Chen, Y.; Wang, G.; Song, L.; Shen, X.; Wang, J.; Huo, J.; Wang, R.; Xu, T.; Dai, S.; Nie, Q., Unraveling the crystallization kinetics of supercooled liquid GeTe by ultrafast calorimetry. *Cryst. Growth Des.* **2017,** *17*, 3687-3693.
44. Chen, B.; de Wal, D.; Ten Brink, G. H.; Palasantzas, G.; Kooi, B. J., Resolving crystallization kinetics of GeTe phase-change nanoparticles by ultrafast calorimetry. *Cryst. Growth Des.* **2018,** *18*, 1041-1046.
45. Chen, B.; Momand, J.; Vermeulen, P. A.; Kooi, B. J., Crystallization kinetics of supercooled liquid Ge–Sb based on ultrafast calorimetry. *Cryst. Growth Des.* **2016,** *16*, 242-248.
46. Ediger, M. D.; Harrowell, P.; Yu, L., Crystal growth kinetics exhibit a fragility-dependent decoupling from viscosity. *J. Chem. Phys.* **2008,** *128*, 034709.
47. Thompson, C. V.; Spaepen, F., On the approximation of the free energy change on crystallization. *Acta Metall.* **1979,** *27*, 1855-1859.
48. Mauro, J. C.; Yue, Y.; Ellison, A. J.; Gupta, P. K.; Allan, D. C., Viscosity of glass-forming liquids. *Proc. Natl. Acad. Sci. U.S.A.* **2009,** *106*, 19780-19784.
49. Scherer, G. W., Editorial comments on a paper by Gordon S. Fulcher. *J. Am. Ceram. Soc.* **1992,** *75*, 1060-1062.
50. Avramov, I.; Milchev, A., Effect of disorder on diffusion and viscosity in condensed systems. *J. Non-Cryst. Solids* **1988,** *104*, 253-260.
51. Cohen, M. H.; Grest, G., Liquid-glass transition, a free-volume approach. *Phys. Rev. B* **1979,** *20*, 1077.
52. Gupta, P. K.; Mauro, J. C., Composition dependence of glass transition temperature and fragility. I. A topological model incorporating temperature-dependent constraints. *J. Chem. Phys.* **2009,** *130*, 094503.
53. Sosso, G. C.; Behler, J.; Bernasconi, M., Breakdown of Stokes–Einstein relation in the supercooled liquid state of phase change materials. *Phys. Status Solidi B* **2012,** *249*, 1880-1885.
54. https://www.mt.com/us/en/home/supportive_content/matchar_apps/MatChar_UC364.html (accessed May 2023).

Table of Contents Graphic